JJBS

Volume 16, Number 3,September 2023
ISSN 1995-6673
Pages 389 – 401
https://doi.org/10.54319/jjbs/160302

Jordan Journal of Biological Sciences

Molecular Simulations of *Moringa oleifera* Phytochemicals as Potential Antagonists of the Proinflammatory NF-κB p50 Transcription Factor

Kathleen Cole C. Tung[1], Romeric F. Pobre[1], Glenn G. Oyong[2,*]

[1]*Department of Physics, De La Salle University, 2401 Taft Avenue, Manila 0922, Philippines;* [2]*Molecular Science Unit Laboratory, Center for Natural Science and Environmental Research, De La Salle University, 2401 Taft Avenue, Manila 0922, Philippines*

Received: July 16, 2022; Revised: January 2, 2023; Accepted: January 25, 2023

Abstract

This study conducted an in silico approach to determine which among the known *Moringa oleifera* phytochemicals demonstrate the most comparable anti-inflammatory activity compared to dexamethasone. Initial screening for druglikeness was performed using Lipinski's rule of five while the ADMET (Absorption, Distribution, Metabolism, Excretion, and Toxicity) properties were investigated. Molecular docking analysis via AutoDock Vina revealed that pterygospermin demonstrated the strongest binding affinity to the target NF-κB p50 (−5.0 kcal/mol), higher than dexamethasone (−4.8 kcal/mol). PharmaGist also provided an overview of the structural features of pterygospermin that could ascertain binding interaction with NF-κB p50. Molecular dynamics simulation using CABS-flex strongly suggested that pterygospermin can stably bind to NF-κB p50 as evidenced by the minimal root mean square fluctuations between the apo and bound structures ($p = 0.4595$). These results suggest that pterygospermin can be a candidate inhibitor of NF-κB p50. Screening for the anti-inflammatory activity of *M. oleifera* leaves, pod, and seed aqueous extract on lipopolysaccharide-induced human THP-1 macrophage cells afforded significant downregulation of proinflammatory *IL1-β* and *TNF-α* transcripts via qRT-PCR ($p < 0.0001$) when compared to non-induced controls. Results from *in silico* studies revealed that *Moringa oleifera* can be a potential source of novel phytochemicals capable of targeting NF-κB and thus impede inflammation.

Keywords: anti-inflammatory, *Moringa oleifera*, in silico, NF-κB p50, phytochemicals

1. Introduction

The ideal, rapid, and short-lived inflammatory response can be classified as acute inflammation; one of two types of inflammation that ultimately allows tissues to return to a state of balance and, consequently, the dissipation of signs and symptoms (Panigrahy *et al.*, 2021). However, the presence of certain social, psychological, environmental, and biological factors can prevent the resolution of acute inflammation, thereby promoting progression to low-grade, non-infective, systemic chronic inflammation (Furman *et al.*, 2019). This condition may entail several months to years riddled with pain, chronic fatigue, insomnia, mood disorders, gastrointestinal complications, and/or frequent infections (Pahwa *et al.*, 2020). Most of the common triggers for low-grade, systemic chronic inflammation are well-integrated into the lifestyle of most individuals (Thompson *et al.*, 2015; Walker *et al*., 2020).

Systemic chronic inflammation (SCI) has been linked to a wide array of disability-causing diseases, including type 2 diabetes mellitus (DM2), cardiovascular disease (CVD), cancer, hypertension, chronic kidney disease, chronic fatty liver disease, sarcopenia, osteoporosis, neurodegenerative diseases, and autoimmune diseases (Furman et al., 2019). Over time, SCI ultimately causes fatalities in tissues and organs, including oxidative stress (Ferrucci and Fabbri, 2018), as well as elevated levels of high-sensitivity C-reactive protein (CRP) inflammatory marker in the blood (Ridker, 2016). SCI consistently triggers the immune cells to either leak out and interfere with insulin in DM2 or induce the cascade to cause fats, cholesterol, and wastes to form plaques that can clog blood vessels in CVD (Lesica, 2017). Prevention is a much better option than cure. However, certain reports implicate that lifestyle interventions in developing countries are plausible only in dietary changes but not substantial for physical inactivity (Sarrafzadegan *et al*., 2009). In addition, occupational hazards which promote consistent exposure to xenobiotics (e.g. mining companies, factory workers) and disrupted circadian rhythms (e.g. call center agents, healthcare workers, college students) can cause chronic stress that weakens the immune system.

Acute and chronic inflammation are often managed with non-steroidal anti-inflammatory drugs (NSAIDs) or corticosteroids. However, these conventional drugs are associated with many adverse effects, especially with long-term use. Moreover, some of these drugs are expensive and not accessible in rural areas which constitute the majority of the population anywhere (Ma *et al*., 2020). This is the reason why around 80% of the population in developing countries has utilized plants as traditional

* Corresponding author. e-mail: glenn.oyong@dlsu.edu.ph.

medicine for health (Adedapo *et al*., 2015). In the Philippines, the Department of Health (DOH) endorses the use of safe, effective, and scientifically validated medicinal plants through the Philippine Institute of Traditional Alternative Health Care (PITAHC) as mandated by Republic Act No. 8423 that was passed in 1997 (Pangalangan, 2013).

Moringa, also called drumstick tree, is a medicinal plant indigenous to South Asia, mainly in the Himalayas, and is now widely distributed in Afghanistan, Nepal, Bangladesh, Sri Lanka, South and Central America, West Indies, the Philippines, and Cambodia (Bhattacharya *et al.*, 2018). *Moringa oleifera* is the most well-studied among the thirteen species of the family Moringaceae. It is believed that *M. oleifera* was first introduced in the Philippines by seamen traveling along the Nao de China route from Manila to Acapulco (Velázquez-Zavala *et al*., 2016). This fast-growing, drought-resistant tree has been deemed "miraculous" as all of its parts, from the leaves to the roots, have been used for food and medicinal purposes (Velázquez-Zavala *et al*., 2016; Olson *et al*., 2016). Its diverse bioactivity is commonly attributed to the phytochemicals that these plants produce to protect themselves from bacteria, viruses, and fungi. Furthermore, traditional medicine asserts *Moringa oleifera* is beneficial for asthma, headaches, digestive disorders, fevers, rheumatism, and inflammation in addition to its nutritional content. Healing properties are mainly due to the presence of several phytochemicals that have antioxidant, antihypertensive, diuretic, analgesic, anticancer, anti-diabetic, antimicrobial, and anti-inflammatory properties (Gopalakrishnan *et al*., 2016; Padayachee and Baijnath, 2020).

A number of *in vivo* and *in vitro* studies indicate that *M. oleifera* has an inhibitory effect on inflammation. A number of in vivo and in vitro studies indicate that *M. oleifera* has an inhibitory effect on inflammation. Studies conducted in vivo to treat induced conditions in mouse and rat models explored the anti-inflammatory and antinociceptive spectrum of *M. oleifera* extracts (Jaja-Chimedza *et al*., 2017; Martínez-González *et al*., 2017; Cretella *et al*., 2020). Meanwhile, *in vitro* studies have examined the anti-inflammatory activity of *M. oleifera* extracts by quantifying proinflammatory cytokines and measuring nitric oxide production in RAW 264.7 or J774A.1 murine macrophage cells in culture (Coppin et al., 2013; Arulselvan *et al*., 2016; Avilés-Gaxiola *et al*., 2021). In general, these studies demonstrated that NF-κB signaling was suppressed through the effective inhibition of inflammatory mediators like cyclooxygenase-2, nitric oxide synthase, and NF-κB expression as well as the upregulated expression of IκBα, the inhibitor of κB, which prevented NF-κB from translocating into the nucleus. These studies conducted consistent efforts in developing an NF-κB signaling inhibitor with therapeutic benefits that would far outweigh its risks. Thus, computer-aided drug design is a practical and cost-effective tool that could predict the potential of different phytochemicals to be developed as potential drugs for clinical use. This study, therefore, proposed an in silico approach to analyzing and identifying the major phytochemicals of *M. oleifera* that can potentially be used as an alternative drug for the treatment of inflammation.

2. Materials and Methods

2.1. Retrieval and Preparation of the NF-κB p50 Target Protein

The three-dimensional (3D) structure of the NF-κB p50 homodimer bound to DNA (PDB ID: 1SVC) was downloaded from the Protein Data Bank (RCSB PDB, https://www.rcsb.org/, accessed on 6 June 2022) and saved as a pdb file (Müller *et al.*, 1995). The 3D structure was modified via BIOVIA Discovery Studio Visualizer v21.1.0.20298 (Dassault Systèmes, Waltham, CA, USA) by removing the heteroatoms and water molecules surrounding the structure. The ligand binding site was defined using the DNA interacting with the NF-κB p50 protein by incorporating a structure-based design (SBD) site sphere which consisted of grid parameters set as center-x-coordinate = 27.79, center-y-coordinate = 30.85, center-z-coordinate = 27.70, and x-, y-, z- size = 20. Lastly, the DNA molecule was deleted from the complex, and the resulting apo (unbound) structure of NF-κB p50 was saved as a pdb file.

Further modifications including the addition of polar hydrogen, Kollman charges, and AutoDock4 atom types on the structure of the protein were done using AutoDock Tools (ADT) v.1.5.6 (Scripps Research, CA, USA) and the resulting structure was saved as a pdbqt file (Morris *et al*., 2009). Finally, the modified NF-κB p50 structure was verified for structural integrity using ERRAT (MacArthur *et al*., 1994) and Verify3D (Bowie *et al*., 1991; Lüthy *et al.*, 1992) via SAVES v.6.0 server (UCLA-DOE, Los Angeles, CA, USA, https://saves.mbi.ucla.edu/, accessed on 6 June 2022), and Ramachandran plot (Anderson *et al*., 2005) via ZLAB (UMass Chan Medical School, Worcester, MA, USA, https://zlab.umassmed.edu/bu/rama/, accessed on 6 June 2022).

2.2. Retrieval and Preparation of Ligands

The phytochemicals of *M. oleifera* were retrieved from the curated database, Indian Medicinal Plants, Phytochemistry, and Therapeutics (IMPPAT 1.0) – a non-redundant in silico library with over 9000 phytochemicals identified from medicinal plants. IMPPAT also introduces 960 druggable phytochemicals that are great candidates for prospective drugs and has no similarities to existing FDA-approved drugs (Mohanraj *et al*., 2018). A total of 15 compounds were available for *M. oleifera* in the Phytochemical Composition section with curated identifiers, names, and references. All 15 structures were downloaded as pdb files from the Phytochemical Identifier section of the database. Dexamethasone (DEX) served as the positive ligand control (Nandeesh *et al*., 2018). The sdf structure (CID: 5743) was retrieved from PubChem (https://pubchem.ncbi.nlm.nih.gov/, accessed on 6 June 2022) as an sdf file.

2.3. Druglikeness and ADMET Prediction

All 15 phytochemicals of *M. oleifera* were evaluated based on their druglikeness via ADMETlab 2.0 (Computational Biology & Drug Design Group, Central South University, Hunan, China, https://admet.scbdd.com/, accessed on 7 June 2022) (Dong *et al*., 2018). Screening criteria is based on Lipinski's rule of five, i.e. a phytochemical is only considered a potential drug

candidate for molecular docking analysis if it does not violate more than one of the following criteria: (1) number of hydrogen bond donors ≤ 5; (2) number of hydrogen bond acceptors ≤ 10; (3) molecular weight is ≤ 500 Da; and (4) Log P ≤ 5 (Lipinski *et al*., 2001). Veber *et al*. (2002) also introduced (5) TPSA ≤ 140Å^2 as the fifth rule that should be considered when assessing the druglikeness of a compound. The isomeric simplified molecular input line entry system (SMILES) of each phytochemical was obtained from PubChem by searching for the provided identifier on IMPPAT. These SMILES structures are submitted to the ADMETlab server. Similarly, further screening was conducted on these phytochemicals by submitting their isomeric SMILES for systematic absorption, distribution, metabolism, excretion, and toxicity (ADMET) assessment. The results were visualized and analyzed via a heatmap created with GraphPad Prism v.9.0.0 for Windows GraphPad Software, San Diego, CA, USA, www.graphpad.com).

2.4. Conversion of Ligands to Dockable Format

The phytochemicals of *M. oleifera* that passed the druglikeness evaluation and ADMET analysis, as well as the reference drug DEX, were checked for stereochemical properties and converted from pdb and sdf to pdbqt using Open Babel GUI v.2.4.1 (GPL v2, SourceForge, San Diego, CA, USA, https://sourceforge.net/projects/openbabel/), accessed on 6 June 2022) (O'Boyle *et al*., 2011). Their structural validity was also checked using BIOVIA Discovery Studio Visualizer.

2.5. Molecular Docking Analysis

Each of the dockable ligands that passed the druglikeness evaluation was individually paired with NF-κB p50. Using AutoDock Vina v.1.2.0. (Scripps Research, CA, USA) (Trott *et al*., 2010), docking was performed by applying the previously determined binding site configuration defined as the center (x = 27.79, y = 30.85, z = 27.70) and size (x = 20, y = 20, z =20) coordinates. The exhaustiveness was left at a default level of 8. After running the command, AutoDock Vina performed an exhaustive series of docking calculations based on the defined binding site by allowing flexibility for the ligands but keeping the NF-κB p50 rigid. Results from the molecular docking analysis were presented as a cluster based on the spatial overlapping of the resulting poses. In each cluster, the pose with the lowest binding energy was selected as its representative. These docking calculations were then repeated thrice (a total of three trials) to obtain the most recurring value for binding energy. These values were then tabulated and ranked. The compound which afforded the lowest binding energy than the positive control DEX was selected for further visualization and analysis using BIOVIA Discovery Studio Visualizer.

2.6. Pharmacophore Modeling

The best binding compound and the positive control were uploaded as a mol2 file to the PharmaGist web server (https://bioinfo3d.cs.tau.ac.il/PharmaGist/php.php, accessed on 8 June 2022) (Inbar *et al*., 2007; Schneidman-Duhovny *et al*., 2008), which determined their pharmacophore features including hydrogen bond donors, hydrogen bond acceptors, hydrophobic atoms, aromatic rings, positively ionizable groups, and negatively ionizable groups. These were visualized with location constraints and vector aromatic ring features using BIOVIA Discovery Studio Visualizer. PharmaGist also provided a score for each pairwise alignment depending on which molecule is considered the key or pivot. The pivot can be set as the ligand with the highest affinity to the receptor (Dror *et al*., 2009). In this case, DEX was the pivot since it is the reference inhibitor.

2.7. Molecular Dynamics Simulation

Due to the known limitations of molecular docking, molecular dynamics simulation was performed to validate the stability of the complex and evaluate the conformational changes in the protein. The pdb files for the bound NF-κB p50-ligand complex and unbound (apo) structures were individually uploaded to the CABS-flex v.2.0 server (http://biocomp.chem.uw.edu.pl/CABSflex2, accessed on 8 June 2022) (Kuriata *et al*., 2018; Jamroz *et al*., 2014). Several models representing the conformational changes occurring in the structure within 0 to 10 nanoseconds were generated. The conformational changes of the apo and bound structures were visualized using BIOVIA Discovery Studio Visualizer by superimposing the different models captured at each nanosecond. To further visualize the differences after ligand binding, the model of the apo structure at 0 nanoseconds was superimposed with the model of the bound structure at 10 nanoseconds. In addition to that, CABS-flex also provided a root mean square fluctuation (RMSF) plot from each amino acid residue before (apo structure) and after binding (bound structure). Paired t-test analysis was applied using GraphPad Prism to determine statistical differences between the models with a significance value set at 0.05.

2.8. Anti-inflammatory Assay against LPS-activated THP-1 Macrophage

2.8.1. Collection and Preparation of Plant Material

The leaves and fruits of *M. oleifera* were collected from the Bureau of Plant Industry, Malate, Manila, Philippines, with the taxonomic identity verified by a resident botanist. A collection of specimens was obtained from and taxonomically identified by the Bureau of Plant Industry, Manila, and was deposited to the Center for Natural Science and Environmental Research at De La Salle University in Manila, Philippines, under voucher number MSUL-XX1902. The leaves and fruits were carefully washed with distilled deionized water three times and air-dried for an hour before carefully removing the leaves from stalks, and separately dissecting the fruit into seeds and pods. The leaves, seeds, and pods were separately ground using liquid nitrogen and the powdered samples were resuspended in complete DMEM cell culture media (described below) to a final of 100 µg/mL concentrations. The aqueous working solutions were filter-sterilized using 0.2 µM syringe filters (Acrodisc, Pall Corp., Port Washington, NY, USA) before further experimentations described below.

2.8.2. Culture of THP-1 monocytes

THP-1 monocytes (ATCC, Manassas, VA, USA) were cultured in 50 mL T-flasks containing complete Dulbecco's Modified Eagle Medium (cDMEM) composed of DMEM with 10% fetal bovine serum and 1X antibiotic antimycotic. All incubation processes were achieved at

37°C with 5% CO_2 in a humidified chamber (Shyu *et al*., 2014). All cell culture reagents were purchased from Invitrogen (Thermo Fisher Scientific, Waltham, MA, USA).

2.8.3. RT-qPCR of Pro-inflammatory IL1-β and TNF-α Transcripts

When 90% confluence was reached, THP-1 cells were harvested and subjected to 0.4% Trypan Blue (Thermo Fisher Scientific, Waltham, MA, USA) exclusion for counting and viability staining. A total of 1 x 105 viable cells/mL were seeded in 100 µL volumes into the wells of a 96-well culture plate. THP-1 differentiation into macrophages was performed by the addition of 160 nM phorbol myristate acetate (PMA) (Sigma-Aldrich, St. Louis, MO, USA) followed by 48 hours incubation. Subsequently, the PMA-induced THP-1 cells (macrophages or Mφ) were stimulated with 100 ng/mL lipopolysaccharide (LPS) (*Escherichia coli* O111:B4, Sigma-Aldrich, St. Louis, MO, USA) for one hour (Shyu *et al*., 2014).

The assay set-up consisted of the following controls: (A) five negative controls – (1) THP-1 cells only (non-differentiated); (2) PMA-induced THP-1 cells (Mφ); and (3–5) PMA-induced THP-1 cells (Mφ) treated with *M. oleifera* leaves, seed, and pod aqueous extracts, respectively; and (B) positive control which consisted of PMA-induced THP-1 cells (Mφ) stimulated with LPS. The treatment set-up was composed of (1–3) PMA-induced THP-1 cells activated by LPS and treated with *M. oleifera* leaves, seed and pod aqueous extracts, and (4) the anti-inflammatory drug DEX. Treatments were done for 30 minutes of incubation. The treatment concentrations of *M. oleifera* extract used were less than the IC_{50} (µg/mL), more precisely IC_{40}, as determined by a previous cytotoxicity test on THP-1 cells (data not shown). The IC_{50} values for the leaf, seed, and pod extracts were 4.65, 7.32, and 8.47 µg/mL, respectively. These IC_{50} values were used to compute the final IC_{40} (sub-IC_{50}) treatment concentrations, yielding values of 3.10, 4.88, and 5.65 µg/mL, respectively. In order to obtain enough cells for gene expression investigation, IC_{40} values were used to maximize the number of viable cells remaining after treatment exposure (Shyu *et al*., 2014). The treatment concentration of DEX was set at 10 µM (~3.925 µg/mL) (Gao *et al*., 2022). All set-ups were accomplished in three replicates. After 30 minutes, 30 µL of RNAlater reagent (Thermo Fisher Scientific, Waltham, MA, USA) was added into each well followed by total RNA extraction using TRIzol kit (Thermo Fisher Scientific, Waltham, MA, USA) following the manufacturer's instructions.

RT-qPCR reactions were performed using Rotor-Gene Q (Qiagen, Germantown, MD, USA) in 20 µL volumes containing: 1X KAPA SYBR FAST One-Step reagent (1X KAPA RT and 1X KAPA SYBR qPCR Master Mix) (Sigma-Aldrich, St. Louis, MO, USA), 10 µM each of forward and reverse primers, nuclease-free water, and 1.0 µL RNA template (50 µg/mL). The primer pair sequences for *IL1-β* were 5'-ATG AAG TGC TCC TTC CAG GAC CTG-3' (forward) and 5'-CCT GGA GTG GAG AGC TTC AGT T-3' (reverse); while for *TNF-α* were 5'-GGA CGT GGA GCT GGC CGA GG-3' (forward) and 5'-TGG GAG TAG ATG AGG TAC AGG CCC-3' (reverse) (Bjorkbacka *et al*., 2004). The PCR profile conditions were as follows: preliminary cDNA synthesis at 50°C for 3 minutes, followed by cDNA amplification of 40 cycles set at 95°C for 20 seconds, 50°C for 40 seconds, and 72°C for 20 seconds. Confirmation of amplified signals was double-checked after high-resolution melting curve analysis set at increments of 72°C to 95°C. Quantification was interpreted as relative fold gene expression ($2^{-\Delta\Delta Ct}$) normalized using the human GAPDH housekeeping control.

2.8.4. Statistical Analysis

Fold gene expression values were presented as mean ± SD. To ascertain the differences between the different treatments, one-way ANOVA with Dunnett's multiple comparisons test integrated within GraphPad Prism was applied, with the level of significance set at 0.05.

3. Results

3.1. Druglikeness and ADMET Evaluation

All 15 *M. oleifera* phytochemicals retrieved from the IMPPAT 1.0 database are presented in Table 1 including their most abundant organ distribution (Abd Rani *et al*., 2018).

Table 1. List of fifteen *M. oleifera* phytochemicals retrieved from the IMPPAT 1.0 database.

No.	Phytochemical Name	Plant Part Abundance
1	28-isoavenasterol acetate	Seed
2	indole acetonitrile	Not listed
3	arachidic acid	Roots
4	benzyl isothiocyanate	Leaves, seeds
5	benzylamine	Aerial
6	DL-alanine-15N	Leaves
7	DL-arginine	Leaves
8	indole-3-acetic acid	Not listed
9	isocoumarin	Not listed
10	ascorbic acid	Leaves, Seeds, Pods
11	maltotriose	Leaves
12	pterygospermin	Seeds
13	SCHEMBL13324298	Not listed
14	tocopherols	Leaves
15	vanillin	Leaves, fruits, seeds

All phytocompounds passed Lipinski's rule of five (RO5) except maltotriose which violated four conditions (Table 2). Meanwhile, results for ADMET were presented as heatmap property distribution depicted in Figure 1.

Table 2. Druglikeness properties of *M. oleifera* phytochemicals based on Lipinski's rule of five: MW = molecular weight; HBD = hydrogen bond donor; HBA = hydrogen bond acceptor; LogP = lipophilicity TPSA = topological polar surface area). Shaded values correspond to violations of the rule.

No.	Phytocompound	MW (g/mol) ≤ 500	HBD ≤ 5	HBA≤ 10	LogP≤ 5	TPSA (Å^2)≤ 140	Druggability
1	28-isoavenasterol acetate	468.766	0	2	8.906	26.30	Pass
2	indole acetonitrile	156.188	1	1	2.234	39.58	Pass
3	arachidic acid	312.538	1	1	7.113	37.30	Pass
4	benzyl isothiocyanate	149.218	0	2	2.289	12.36	Pass
5	benzylamine	107.156	1	1	1.145	26.02	Pass
6	DL-alanine-15N	90.087	2	2	-0.582	63.32	Pass
7	DL-arginine	175.212	4	2	-5.519	133.78	Pass
8	indole-3-acetic acid	175.187	2	1	1.795	53.09	Pass
9	isocoumarin	194.186	2	4	0.984	66.76	Pass
10	ascorbic acid	176.124	4	6	-1.407	107.22	Pass
11	maltotriose	504.438	11	16	-7.573	268.68	Fail
12	pterygospermin	406.532	0	4	4.14	24.94	Pass
13	SCHEMBL13324298	398.675	1	1	7.555	20.23	Pass
14	tocopherols	416.69	1	2	8.532	29.46	Pass
15	vanillin	152.149	1	3	1.213	46.53	Pass

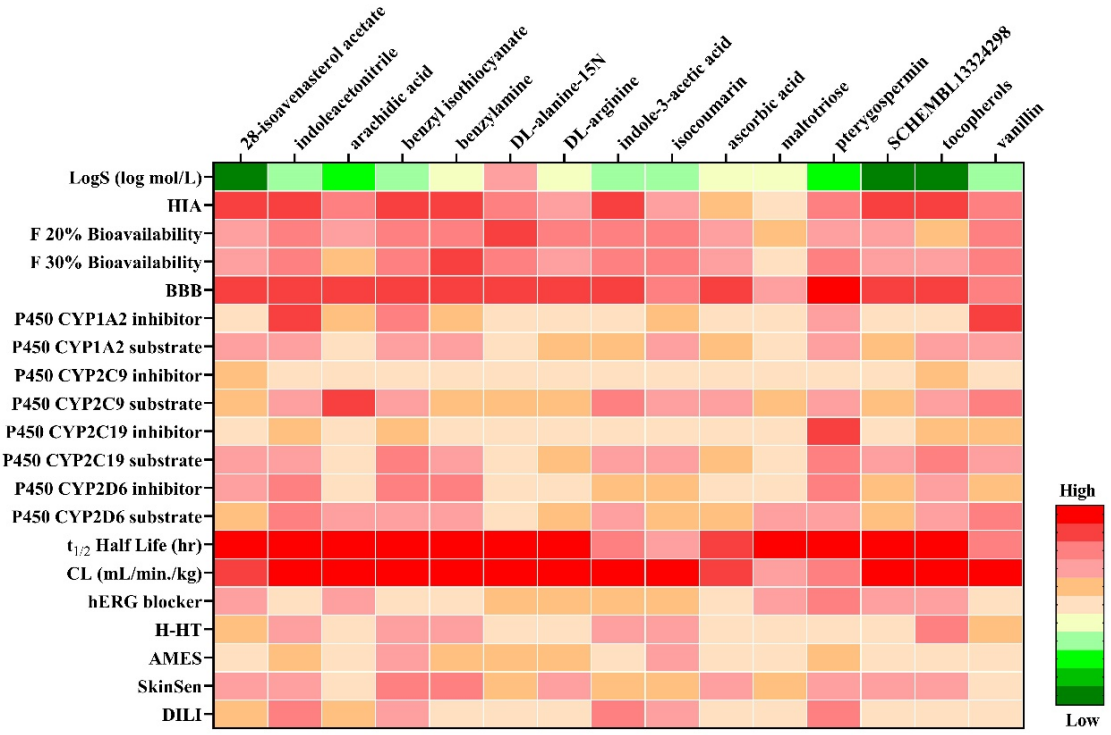

Figure 1. Heatmap for the ADMET property distribution of *M. oleifera* phytocompounds. LogS = solubility; HIA = Human Intestinal Absorption; BBB = Blood-Brain Barrier; CL = Clearance Rate; H-HT = Human Hepatotoxicity; AMES = Ames Mutagenicity; SkinSen = Skin Sensitization; DILI = Drug-Induced Liver Injury). LogS, HIA, bioavailability, and BBB are predictive properties of a drug's absorption; cytochrome P450 inhibitors and substrates are predictive properties of metabolism; half-life and CL are predictive properties of excretion; and hERG blocker, H-HT, AMES, SkinSen, and DILI are predictive properties of toxicity.

3.2. Structural Validity of Prepared NF-κB p50 Protein

The prepared structure of NF-κB p50 was verified for structural validity via Ramachandran plot, ERRAT, and Verify3D (Figure 2A-2C). Results from the Ramachandran Plot Zlab server showed that 251 amino acid residues (94.361%) were in the highly preferred observations (Figure 2A). It also showed that 13 amino acid residues (4.887%) were in the preferred observations while only 2 amino acid residues (0.752%), Tyr90 and Ser81, were in the questionable observations. This confirmed that the prepared protein possesses a good model structure since over 90% of the protein residues are in the most favored or core regions in the Ramachandran plot (Balaji *et al.*, 2006). The 3D folding of the prepared NF-κB p50 protein was assessed by VERIFY3D using the protein's own amino acid sequence to test the accuracy of the 3D model, also known as the 3D-1D profile (AboMeireles *et al.*, 1992). According to Figure 2B, 99.04% of the residues afforded an averaged 3D-1D score ≥ 0.2 and at least 80% of the amino acids scored ≥ 0.2 in the 3D/1D profile. ERRAT differentiates between correctly and incorrectly

determined regions of protein structures based on characteristic atomic interaction and is expressed as the percentage of the protein for which the calculated error value falls below the 95% rejection limit. As shown in Figure 2C, the overall quality factor of the modified NF-κB p50 protein is 80.537%. Thus, the prepared NF-κB p50 protein has passed all verification methods of structural validity for molecular docking analysis.

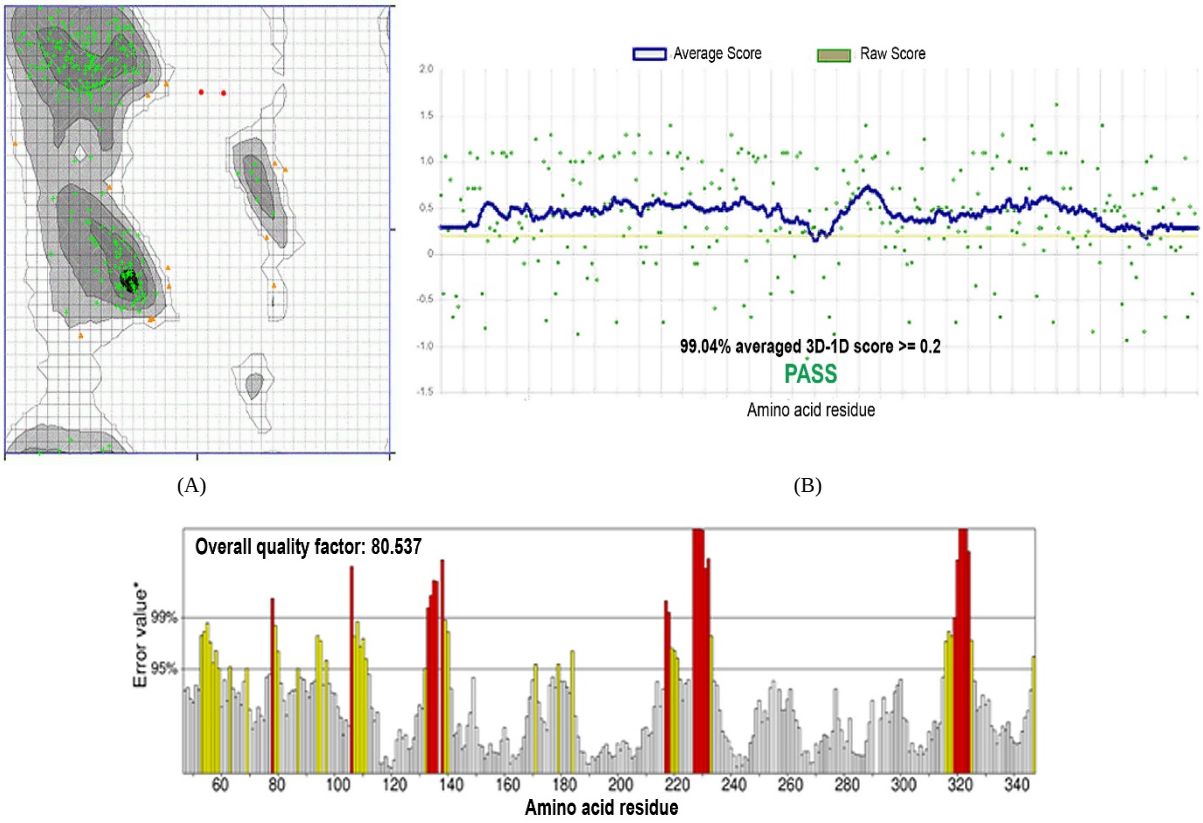

Figure 2. (A) Ramachandran plot of the modified NF-kB p50 protein with highly preferred observations (green), preferred observations (orange), and questionable observations (red). (B) VERIFY3D showing the averaged 3D-1D score >= 2.0 and 99.04 % pass score. (C) ERRAT which shows that the overall quality factor falls below the 95% rejection limit.

3.3. Molecular Docking Results

Based on the results of the druglikeness evaluation (Table 2), 14 out of 15 *M. oleifera* phytochemicals from the IMPPAT database were subjected to docking analysis. DEX was also used as a reference inhibitor of the target protein NF-κB p50. For each pair (protein and ligand), AutoDock Vina performed docking calculations to determine the binding energy of the protein-ligand complex. Results from these docking calculations are shown in Table 3.

Table 3. Binding energies of the 14 phytochemicals and dexamethasone reference compound to the NF-κB p50 binding site.

Compound	PubChem CID	Phytochemistry	Binding Energy (kcal/mol)
Dexamethasone (control)	5743	corticosteroid	–4.8
Pterygospermin	72201063	benzenoid (benzene/substituted derivative)	–5.0
28-isoavenasterol acetate	91746804	lipid and lipid-like (triterpenoid)	–4.7
isocoumarin, 3,4-dihydro-4,8-dihydroxy-3-methyl-	169539	organoheterocyclic compound (2-benzopyran)	–4.4
SCHEMBL13324298	23724573	lipid and lipid-like molecules (ergostane steroid)	–4.4
2-(1H-indol-2-yl)acetonitrile	169731	organoheterocyclic compound (indole)	–4.2
indole-3-acetic acid	802	organoheterocyclic (indolyl carboxylic acid derivative)	–4.1
DL-arginine	1549073	amino acid	–4.0
Tocopherols	14986	lipid and lipid-like (Quinone/Hydroquinone)	–3.9
arachidic acid	10467	lipid and lipid-like (fatty acid)	–3.6
Vanillin	1183	benzenoid (methoxy phenol)	–3.6
ascorbic acid	54670067	organoheterocyclic (furanone)	–3.5
benzyl isothiocyanate	2346	benzenoid (benzene/substituted derivative)	–3.4
Benzylamine	7504	benzenoid (phenylmethylamine)	–3.2
DL-alanine-15N	51283	amino acid	–2.9

Pterygospermin topped the lowest score (–5.0 kcal/mol) for binding energy (highest affinity) and the docked configuration with NF-κB p50 is shown in Figure 3A-3F.

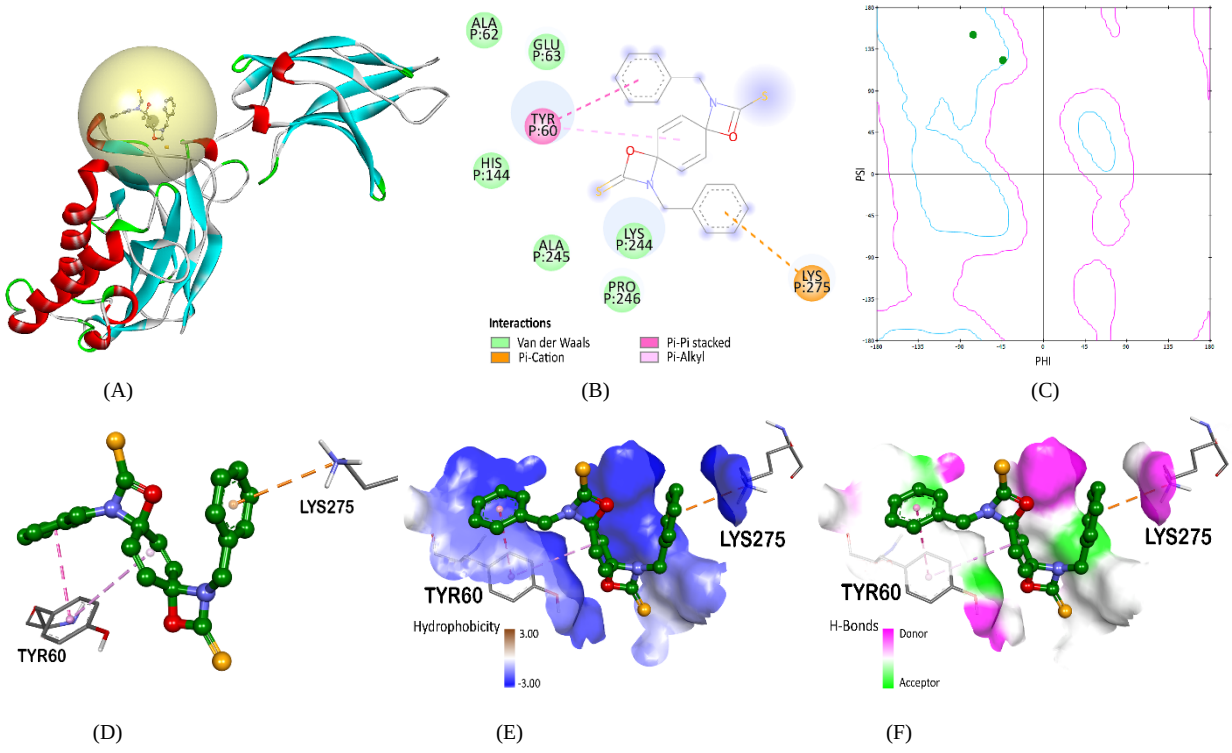

(A) (B) (C)

(D) (E) (F)

Figure 3. Binding interactions of NF-κB p50 and pterygospermin: (A) 3D visualization of pterygospermin docked in NF-κB p50 within the ligand binding site (yellow sphere); (B) 2D display of pterygospermin-NF-κB p50 interactions; (C) Ramachandran plot of ligand-interacting amino acid residues; (D) 3D display of pterygospermin-NF-κB p50 interactions; (E) hydrogen bond surface of binding pocket; and (F) hydrophobicity surface of the binding pocket.

3.4. Pharmacophore Features and Pairwise Alignment Score

Pharmacophore analysis (Table 4) confirmed that pterygospermin has four acceptors (two oxygen and two sulfur atoms) and two aromatic rings that can form hydrogen bonds and non-covalent π-system interactions with NF-κB p50, respectively (Figure 4A). On the other hand, dexamethasone has eleven hydrophobic groups and four acceptors (oxygen atoms) that can interact with NF-κB p50 (Figure 4B). Despite having a pairwise alignment score of 4.51428 which is most likely the result of the shared hydrogen-bond acceptor features, pterygospermin and dexamethasone have been shown to snugly fit in the NF-κB p50 binding pocket (Figure 4C).

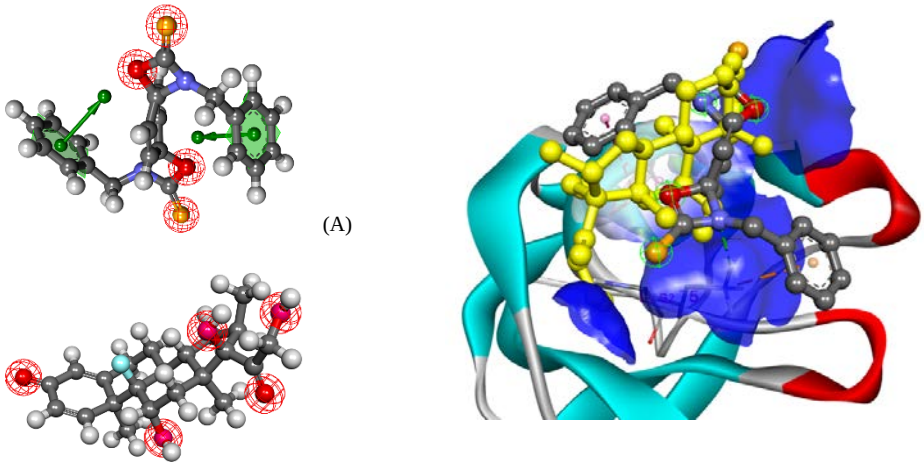

(A) (B) (C)

Figure 4. Comparison of 3D models showing the pharmacophore features of (A) pterygospermin and (B) dexamethasone. Each color corresponds to the hydrogen bond donors (orange), hydrogen bond acceptors (red), and aromatic rings (green). Note that some oxygen atoms in dexamethasone act as both hydrogen bond donors and acceptors. (C) Superimposed structures of pterygospermin (gray) and dexamethasone (yellow) showing both compounds fitting inside the NF-κB p50 binding pocket.

Table 4. Pharmacophore physico-chemical features of dexamethasone and pterygospermin.

Molecule	Atoms	Features	Aromatic	Hydrophobic	Donors	Acceptors
dexamethasone	57	19	0	11	3	5
pterygospermin	46	6	2	0	0	4

3.5. Molecular Dynamics Simulation

Minimal fluctuations (0–7.2Å) were observed between the pterygospermin-bound NF-κB p50 compared with the apo (non-bound) structure (Figure 5A). The superimposed multimodel MDS structures across 0 to 10 nanosecond trajectories also affirmed insignificant structural variations when the apo (Figure 5B) is compared with the pterygospermin-bound structure (Figure 5C) which can also be seen with the overlayed structures of the apo at 0 nanoseconds and the bound structure at 10 nanoseconds (Figure 5D).

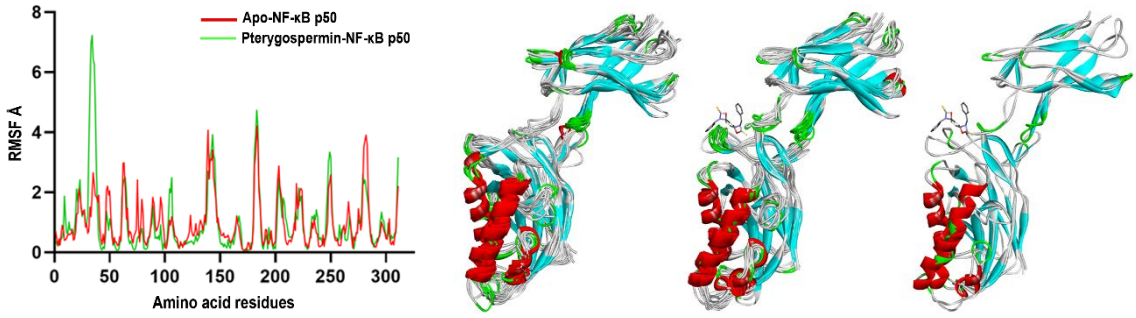

(A) (B) (C) (D)

Figure 5. Molecular dynamics simulation (MDS) comparing the apo and pterygospermin-bound structures of NF-κB p50. (A) RMSF profiles of the amino acid residues of the apo (red) and bound structures (green). Trajectory model superimposition of: (B) apo-NF-κB structures from 0–10 nanoseconds; (C) pterygospermin-NF-κB p50 complexes from 0–10 nanoseconds; and (D) apo structure at 0 nanosecond and pterygospermin-NF-κB p50 at 10 nanoseconds.

3.6. Anti-inflammatory Assay against LPS-activated THP-1 Macrophage

THP-1 cells transformed into macrophages and induced by LPS bacterial antigen were assayed for the expression of *IL1-β* and *TNF-α* transcripts (Figure 6). Figure 7 shows the downregulation of the expression of both proinflammatory cytokine genes brought about by treatment with *M. oleifera* leaves, seed, and pod aqueous extracts.

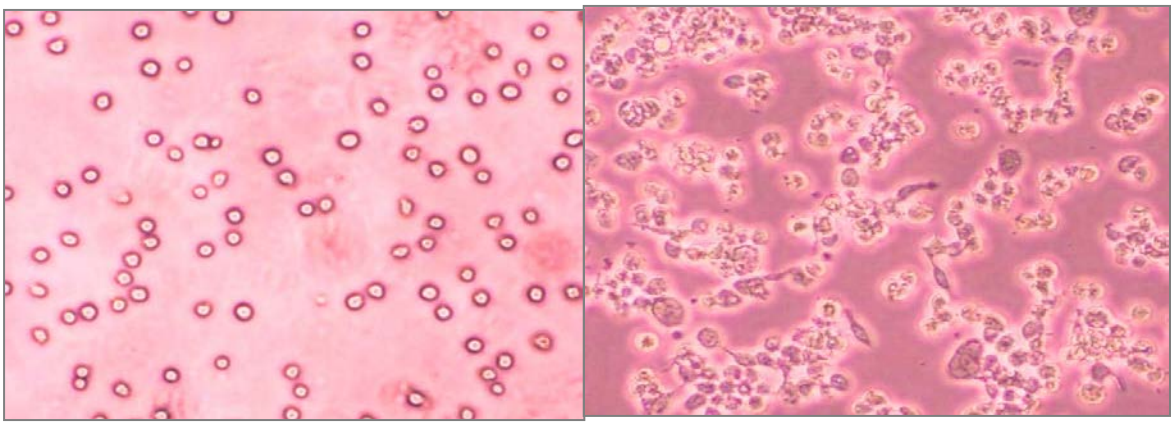

(A) (B)

Figure 6. Phase contrast photomicrographs (200X) of (A) floating THP-1 monocytes and (B) differentiated macrophages which appear enlarged and attached 48 hours after PMA treatment.

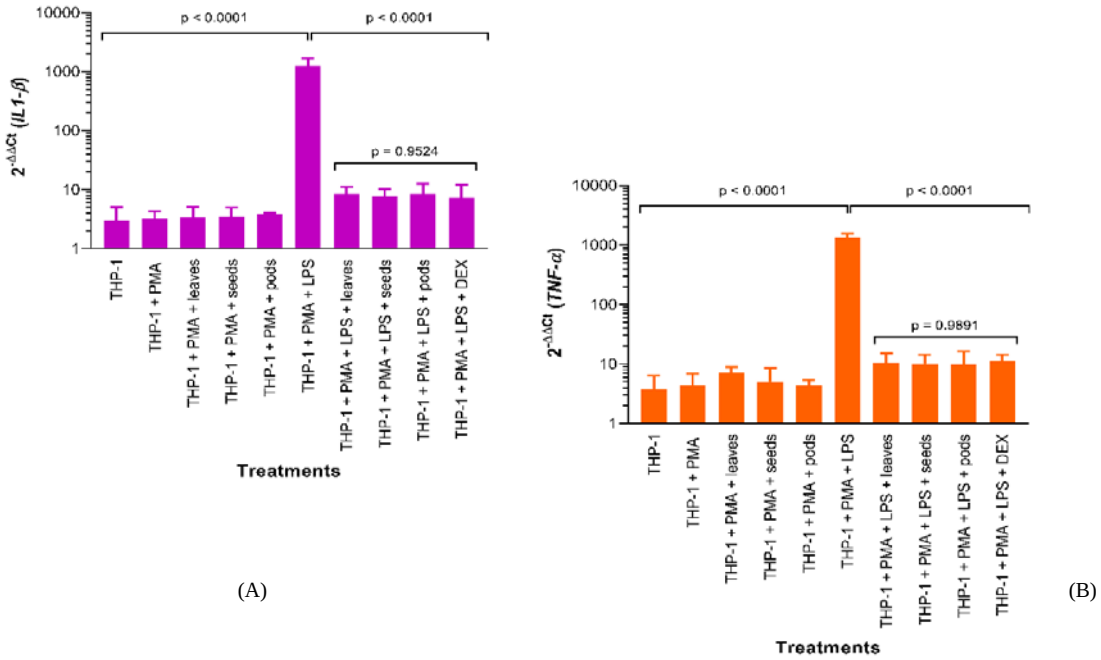

(A) (B)

Figure 7. Relative gene expression ($2^{-\Delta\Delta Ct}$) profiles of (A) *IL-1β* and (B) *TNF-α* cytokine gene transcripts. Significant difference from the control group positive for inflammation afforded an F test of F (9, 20) = 24.60, p < 0.0001 for *IL1-β*, and F (9, 20) = 90.34, p < 0.0001 for *TNF-α*.

4. Discussion

Druglikeness analysis using Lipinski's rule of five (RO5) resulted in all *M. oleifera* phytocompounds passing the criteria except for maltotriose. According to the rule, this could indicate that maltotriose would perform poorly as a drug because of its suboptimal permeability and absorption. More specifically, its molecular weight could mean that the molecule is too large to pass through the cell membrane. It also exceeded the acceptable number of hydrogen bond donors and acceptors which contribute to its enhanced solubility in the blood thereby decreasing its bioavailability and time to effectively permeate membranes and cross the blood-brain barrier. Maltotriose also exceeded the cut-off value for TPSA, which implies that it may be poorly distributed and transported in the body. Despite these, it is important to note that this rule is not a strong indication that maltotriose would perform poorly as a drug during actual in vivo clinical settings. Moreover, ADMET analysis also showed that maltotriose has relatively high solubility and low blood-brain barrier permeability compared to the other phytochemicals (Figure 1). Considering these probabilities, maltotriose was eliminated from the list of phytochemicals that were subjected to subsequent molecular docking simulations with the NF-κB p50 protein.

ADMET analysis of the 14 compounds which showed no RO5 violations deduced high intestinal absorption (HIA), cross the blood-brain barrier (BBB), and high bioavailability (F20%, F30%) properties (Figure 1). However, alanine solely appeared to be highly soluble (LogS). All 14 compounds also indicated a medium-to-high probability of either inhibitors or substrates for P450

CYP-aided drug metabolism. Further analysis also suggested that these compounds may exhibit an average likelihood of exhibiting toxicity albeit with a short half-life and high systemic clearance (CT).

Subsequent Autodock Vina analysis ranked the phytocompounds from the lowest to highest binding energies (Table 3). Note that the values for the binding energy represent the most recurring values after three runs of docking calculations. Results from these calculations revealed that the reference inhibitor DEX had a binding energy of −4.8 kcal/mol. The phytochemicals of *M. oleifera* produced binding energies that ranged from −2.9 kcal/mol to −5.0 kcal/mol. Out of all the phytocompounds, pterygospermin demonstrated the strongest affinity (the lowest binding energy) to NF-κB p50 (−5.0 kcal/mol), whereas DL-alanine-15N showed the weakest (−2.9 kcal/mol). Pterygospermin also displayed a stronger affinity for NF-κB p50 at the DNA binding site than the reference inhibitor DEX which suggests that it could be a possible drug candidate for p50 inhibition, and therefore, potentially ameliorate inflammation. Further analysis of the interactions between pterygospermin and the NF-κB p50 binding site showed only Tyr60 and Lys275 directly interacting with the ligand (Figures 3B, 3D). The Ramachandran plot indicates that Tyr60 and Lys275 are located in the β-sheet structures of NF-κB p50 (Figure 3C). Tyr60 has an aromatic ring that can form hydrophobic interactions with the aromatic ring of pterygospermin via pi (π) stacking. This π–π interaction occurs at a distance of 4.261Å. This is a notable type of non-covalent interaction because it reportedly plays a vital role in the biological recognition and organization of biomolecular structures (Brylinski, 2018). Pi stacking can occur in three different ways: perpendicular, parallel, or eclipsed. A pi-alkyl hydrophobic interaction (5.38Å) between the aromatic ring of Tyr60 and the alkyl group of the non-aromatic ring structure in pterygospermin is also present. There is also a pi-cation electrostatic interaction (4.38Å) between the nitrogen of Lys275 and the second aromatic ring in pterygospermin (Figure 3D).

It is clearly shown that the active pocket amino acids are mostly hydrophilic based on the generated hydrophobicity and H-bond surfaces (Figure 3E, 3F). Further analysis revealed that the formal positively charged nitrogen from Lys275 is the reason for the electrostatic interaction with the negatively charged center of the aromatic ring in pterygospermin. Pi interactions between the protein and the ligand depicted by the pi-alkyl interaction have an edge-to-face configuration. Additionally, the aromatic rings of tyrosine and pterygospermin demonstrated a face-to-face or parallel configuration which is theorized to "correspond to energy minima of comparable depth" (Brylinski, 2018). Paired t-test analysis confirmed that there is no significant difference in the fluctuation of amino acid residues from both unbound NF-κB p50 and pterygospermin-bound NF-κB p50 complex ($p = 0.4595$) after molecular dynamics simulation. These results strongly suggest that pterygospermin can form a stable complex with NF-κB p50 and, therefore, has considerable potential to serve as an anti-inflammatory drug.

This study also investigated the anti-inflammatory activity of *M. oleifera* leaves, seed, and pod aqueous extracts in LPS-stimulated human macrophages. *Figure* 7 shows the downregulation of the expression of both proinflammatory cytokine genes brought about by treatment with the *M. oleifera* extracts. There was a significant decrease or downregulation in the expression of the levels of *IL1-β* ($p < 0.0001$) and *TNF-α* ($p < 0.0001$) proinflammatory cytokine genes in cells exposed to any of the three *M. oleifera* extracts compared to the positive control set-up composed of macrophages stimulated with LPS. Several studies have recently investigated the anti-inflammatory potential of *M. oleifera*. The leaves were discovered to control *TNF-α* and *INF-γ* production in natural killer cells from type 1 diabetes mice models (Lestari *et al*., 2022). The ethanolic leaf extract was also found to promote the ameliorative effects against oxidative stress, inflammation, and apoptosis in CCl_4-induced hepatic encephalopathy (Mahmoud *et* al., 2022) and bisphenol-induced gastric ulcer in mice (Abo-Elsoud *et al*., 2022). The seeds were discovered to contain bioactive compounds with antiviral activity against H1N1 and anti-inflammatory properties by decreasing the levels of TNF-α, IL-6, and IL-1β, in hosts with H1N1 infection (Xiong *et al*., 2022). Additionally, antibacterial and anti-inflammatory activity against *Helicobacter pylori* infections was also ascertained in *M. oleifera* seeds (Sayed *et al*., 2022). Meanwhile, *M. oleifera* pods, together with leaves and seeds, were reported to exhibit medicinal properties including anti-inflammatory, antidiabetic, antineoplastic, antibacterial, and antifungal activities (Anwar *et al*., 2007; Mbikay, 2012; Meireles, *et* al., 2020).

Research that investigated the anti-inflammatory property of *M. oleifera* commonly involved the detection of proinflammatory cytokines in mice models (Sharma *et* al., 2012; Lestari *et al*., 2022; Mahmoud *et* al., 2022; Abo-Elsoud *et al*., 2022). By extensive literature search, this study is the first to report the application of human macrophage cells derived from PMA-transformed THP-1 monocytes for determining the anti-inflammatory activity of *M. oleifera* leaves, pod, and seed aqueous extracts. Furthermore, the significant decrease in the relative gene expression of *IL1-β* and *TNF-α* is directly due to transcriptional level downregulation which can be directly linked to the inactivation of NF-κB. A proposed mechanism is presented in Figure 8. Pterigospermin and other phytochemicals present in *M. oleifera* may have consequentially played pivotal roles in the inhibition of the NF-κB p50 transcription factor domain which may have blocked its binding to the promoter regions of genes specifically coding for proinflammatory cytokines such as *IL1-β* and *TNF-α.* However, this putative mechanism has to be tested and confirmed further by isolating the phytochemicals from the extracts and subjecting them to anti-inflammatory bioassays.

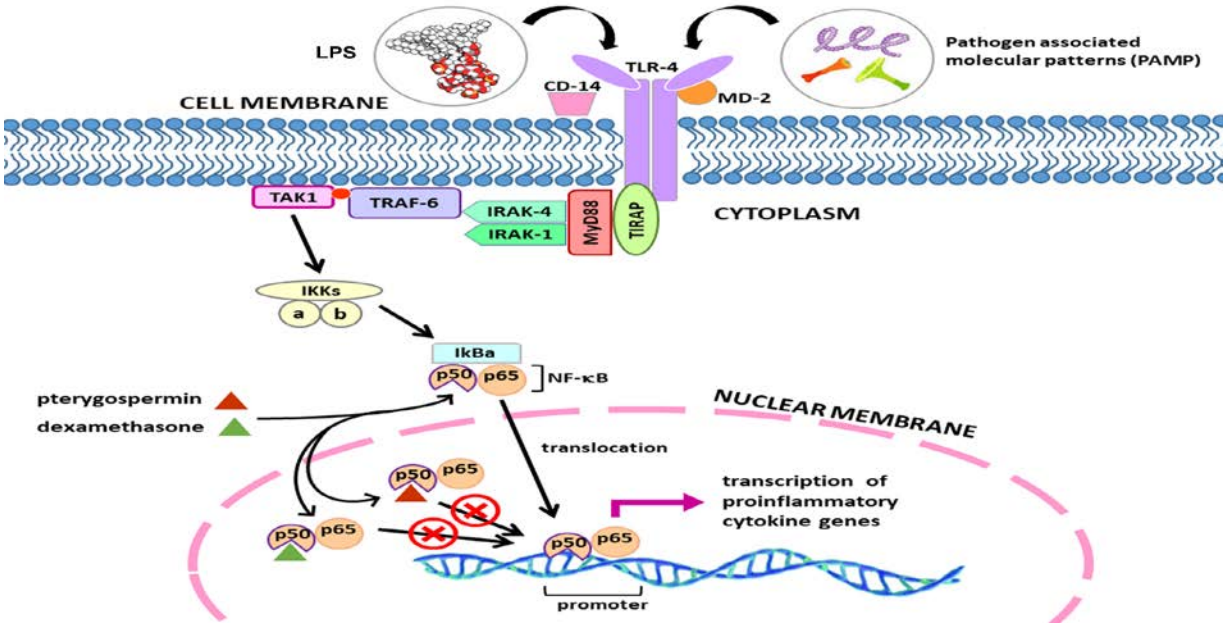

Figure 8. Proposed mechanism of NF-κB p50 antagonism by pterygospermin. The binding of either LPS or PAMP on TLR-4 activates the NF-κB signaling system to promote the transcriptional activation of proinflammatory cytokine gene expression. Pterygospermin is proposed to block the NF-κB p50 DNA binding domain inhibiting downstream cytokine expression.

5. Conclusions

Researchers are prompted to develop a safe and effective drug that can alleviate the signs and symptoms of inflammation. One particular research area of interest is the inhibition of NF-κB – a transcription factor that is widely accepted as a major inflammatory mediator. Most of the drugs in development for NF-κB inhibition are still in their clinical stages. Simultaneously, there is an increasing wealth of research on the anti-inflammatory activity of *M. oleifera*. Its biological activity has been attributed to the numerous phytochemicals that can be extracted and can be potential drug candidates. This study utilized an in silico approach to identify a lead compound among the phytochemicals of *M. oleifera* for potential use as an inhibitory drug against the homodimer NF-κB p50.

Pterygospermin passed the druggability criteria characterized by good absorption properties, moderately high metabolic stability, and median to low toxicity but with high half-life and clearance. Docking analysis on the NF-κB p50 binding pocket afforded the highest binding affinity surpassing dexamethasone, a known anti-inflammatory drug. This suggests the potential of pterygospermin to block the p50 transcription factor from recognizing the promoter regions of proinflammatory cytokine genes. This has been proven in part by the effective downregulation of expression of *IL1-β* and *TNF-α* transcripts after the treatment of LPS-activated macrophages with *M. oleifera* extracts. In conclusion, *M. oleifera* can be a good potential source of pharmaceutical leads capable of inhibiting the NF-κB p50 protein. However, the eventual prevention of the expression of cytokine genes at the transcriptional, and subsequently at the protein levels, warrants further investigation and additional experiments to firmly establish the inhibition of the NF-κB pathway.

Acknowledgments

The authors wish to express thanks to the Department of Physics and the Molecular Science Unit Laboratory–Center for Natural Science and Environmental Research, De La Salle University, Manila.

References

Abd Rani NZ, Hisain K and Kumolosasi E. 2018. *Moringa* genus: A review of phytochemistry and pharmacology. *Front Pharmacol.*, **9(108)**: 1-26.

Abo-Elsoud RAEA, Abdelaziz SAM, Eldaim MAA and Hazzaa SM. 2022. *Moringa oleifera* alcoholic extract protected stomach from bisphenol A-induced gastric ulcer in rats via its anti-oxidant and anti-inflammatory activities. *Environ Sci Pollut Res.*, **29(45)**: 68830-68841.

Adedapo AA, Falayi OO and Oyagbemi AA. 2015. Evaluation of the analgesic, anti-inflammatory, anti-oxidant, phytochemical and toxicological properties of the methanolic leaf extract of commercially processed *Moringa oleifera* in some laboratory animals. *J Basic Clin Physiol Pharmacol.*, **26(5)**: 491-499.

Anderson RJ, Weng Z, Campbell RK and Jiang X. 2005. Main-chain conformational tendencies of amino acids. *Proteins.*, **60(4)**: 679-689.

Anwar F, Latif S, Ashraf M and Gilani AH. 2007. *Moringa oleifera*: A food plant with multiple medicinal uses. *Phytother Res.*, **21(1)**: 17–25.

Arulselvan P, Tan WS, Gothai S, Muniandy K, Fakurazi S, Esa NM, Alarfaj AA and Kumar SS. 2016. Anti-inflammatory potential of ethyl acetate fraction of *Moringa oleifera* in downregulating the NF-κB signaling pathway in lipopolysaccharide-stimulated macrophages. *Molecules.*, **21(11)**: 1-13.

Avilés-Gaxiola S, León-Félix J, Jiménez-Nevárez YB, Angulo-Escalante MA, Ramos-Payán R, Colado-Velázquez JI and Heredia JB. 2021. Antioxidant and anti-inflammatory properties of novel peptides from *Moringa oleifera* Lam. leaves. *S Afr J Bot.*, **141**: 466-473.

Balaji S, Kalpana R and Shapshak P. 2006. Paradigm development: comparative and predictive 3D modeling of HIV-1 Virion Infectivity Factor (VIF). *Bioinformation.*, **1(8)**: 290-309.

Bhattacharya A, Tiwari P, Sahu PR and Kumar S. 2018. A review of the phytochemical and pharmacological characteristics of *Moringa oleifera*. *J Pharm Bioallied Sci*., **10(4)**: 181-191.

Bjorkbacka H, Fitzgerald KA, Huet F, Li X, Gregory JA, Lee MA, Ordija CM, Dowley NE, Golenbock DT and Freeman MW. 2004. The induction of macrophage gene expression by LPS predominantly utilizes Myd88-independent signaling cascades. *Physiol Genomics.*, **19(3)**: 319-330.

Bowie JU, Lüthy R and Eisenberg D. 1991. A method to identify protein sequences that fold into a known three-dimensional structure. *Science*., **253(5016)**: 164-170.

Brylinski M. 2018. Aromatic interactions at the ligand-protein interface: Implications for the development of docking scoring functions. *Chem Biol Drug Des.*, **91(2)**: 380-390.

Coppin JP, Xu Y, Chen H, Pan M, Ho C, Juliani R, Simon JE and Wu Q. 2013. Determination of flavonoids by LC/MS and anti-inflammatory activity in *Moringa oleifera*. *J Funct Foods.*, **5(4)**: 1892-1899.

Cretella ABM, Soley BDS, Pawloski PL, Ruziska RM, Scharf DR, Ascari J, Cabrini DA and Otuki MF. 2020. Expanding the anti-inflammatory potential of *Moringa oleifera*: topical effect of seed oil on skin inflammation and hyperproliferation. *J Ethnopharmacol.*, **23(254)**: 1-12.

Dong J, Wang NN, Yao ZJ, Zhang L, Cheng Y, Ouyang D, Lu AP and Cao DS. 2018. ADMETlab: a platform for systematic ADMET evaluation based on a comprehensively collected ADMET database. *J Cheminform.*, **10(1)**: 1-29.

Dror O, Schneidman-Duhovny D, Inbar Y, Nussinov and Wolfson HJ. 2009. Novel approach for efficient pharmacophore-based virtual screening: method and applications. *J Chem Inf Model.*, **49(10)**: 2333-2343.

Ferrucci L and Fabbri E. 2018. Infammageing: chronic infammation in ageing, cardiovascular disease, and frailty. *Nat Rev Cardiol.*, **15(9)**: 505-522.

Furman D, Campisi J, Verdin E, Carrera-Bastos P, Targ S, Franceschi C, Ferrucci L, Gilroy DW, Fasano A, Miller GW, Miller AH, Mantovani A, Weyand CM, Barzilai N, Goronzy JJ, Rando TA, Effros RB, Lucia A, Kleinstreuer N and Slavich GM. 2019. Chronic inflammation in the etiology of disease across the life span. *Nat Med.*, **25(12)**: 1822-1832.

Gao M, Lee SB, Lee J-E, Kim GJ, Moon J, Nam J-W, Bae J-S, Chin J, Jeon YH and Choi H. 2022. Anti-Inflammatory butenolides from a marine-derived *Streptomyces* sp. 13G036. *Appl Sci.*, **12(9)**: 1-11.

Gopalakrishnan LH, Doriya K and Kumar DS. 2016. *Moringa oleifera*: A review on nutritive importance and its medicinal application. *Food Sci Hum Wellness.*, **5(2)**: 49-56.

Inbar Y, Schneidman-Duhovny D, Dror O, Nussinov R and Wolfson HJ. 2007. Deterministic pharmacophore detection via multiple flexible alignment of drug-like molecules. Proceedings of Research in Computational Molecular Biology, Lecture Notes in Computer Science. Springer Verlag, Germany.

Jaja-Chimedza A, Graf BL, Simmler C, Kim Y, Kuhn P, Pauli GF and Raskin I. 2017. Biochemical characterization and anti-inflammatory properties of an isothiocyanate-enriched moringa (*Moringa oleifera*) seed extract. *PLoS One.*, **12(8)**: 1-21.

Jamroz M, Kolinski A and Kmiecik S. 2014. CABS-flex predictions of protein flexibility compared with NMR ensembles. *Bioinformatics.*, **30(15)**: 2150-2154.

Kuriata A, Gierut AM, Oleniecki T, Ciemny MP, Kolinski A, Kurcinski M and Kmiecik S. 2018. CABS-flex 2.0: a web server for fast simulations of flexibility of protein structures. *Nucleic Acids Res.*, **46(W1)**: W338-W343.

Lesica NA. 2017. Inflammation. In: **Conversation about Healthy Eating**. UCL Press, London, England, pp. 26-38.

Lipinski CA, Lombardo F, Dominy BW and Feeney PJ. 2001. Experimental and computational approaches to estimate solubility and permeability in drug discovery and development settings. *Adv Drug Deliv Rev.*, **46(1-3)**: 3-26.

Lüthy R, Bowie JU and Eisenberg D. 1992. Assessment of protein models with three-dimensional profiles. *Nature.*, **356(6364)**: 83-85.

Ma ZF, Ahmad J, Zhang H, Khan I and Muhammad. 2020. Evaluation of phytochemical and medicinal properties of Moringa (*Moringa oleifera*) as a potential functional food. *S Afr J Bot.*, **129**: 40-46.

Mahmoud MS, El-Kott AF, AlGwaiz HIM and Fathy SM. 2022 Protective effect of *Moringa oleifera* Lam. leaf extract against oxidative stress, inflammation, depression, and apoptosis in a mouse model of hepatic encephalopathy. *Environ Sci Pollut Res Int.*, **29(55)**: 83783-83796.

MacArthur MW, Laskowski RA and Thornton J M. 1994. Knowledge-based validation of protein structure coordinates derived by X-ray crystallography and NMR spectroscopy. *Curr Opin Struct Biol.*, **4(5)**: 731-737.

Martínez-González CL, Martínez L, Martínez-Ortiz EJ, González-Trujano ME, Déciga-Campos M, Ventura-Martínez R and Díaz-Reval I. 2017. *Moringa oleifera*, a species with potential analgesic and anti-inflammatory activities. *Biomed Pharmacother.*, **87**: 482-488.

Mbikay, M. 2012. Therapeutic potential of *Moringa oleifera* leaves in chronic hyperglycemia and dyslipidemia: A review. *Front Pharmacol.*, **3**: 1-24.

Meireles D, Gomes J, Lopes L, Hinzmann M and Machado J. 2020. A review of properties, nutritional and pharmaceutical applications of *Moringa oleifera*: integrative approach on conventional and traditional Asian medicine. *Adv Tradit Med.*, **20(4)**: 495-515.

Mohanraj K, Karthikeyan BS, Vivek-Ananth RP, Chand RPB, Aparna SR, Mangalapandi P and Samal A. 2018. IMPPAT: A curated database of Indian Medicinal Plants, Phytochemistry and Therapeutics. *Sci Rep.*, **8(1)**: 1-17.

Müller CW, Rey FA, Sodeoka M, Verdine GL and Harrison SC. 1995. Structure of the NF-kappa B p50 homodimer bound to DNA. *Nature.*, **373(6512)**: 311–317.

Nandeesh R, Vijayakumar S, Munnolli A, Alreddy A, Veerapur VP, Chandramohan V and Manjunatha E. 2018. Bioactive phenolic fraction of *Citrus maxima* abate lipopolysaccharide-induced sickness behaviour and anorexia in mice: In-silico molecular docking and dynamic studies of biomarkers against NF-κB. *Biomed Pharmacother.*, **108**: 1535–1545.

Lestari ND, Rahmah AC, Adharini WI, Nilamsari RV, Jatmiko NW, Yoga D, Rahayu S and Rifa'i M. 2022. Bioactivity of *Moringa oleifera* and albumin formulation in controlling TNF-α and lFN-γ production by NK cells in mice model type 1 diabetes. *Jordan J Biol Sci.*, **15(2)**: 205-208.

O'Boyle NM, Banck M, James CA, Morley C, Vandermeersch T and Hutchison GR. 2011. Open Babel: An open chemical toolbox. *J Cheminform.*, **3(33)**: 1-14.

Olson ME, Sankaran RP, Fahey JW, Grusak MA, Odee D and Nouman W. 2016. Leaf protein and mineral concentrations across the 'miracle tree' genus *Moringa*. *PLoS One.*, **11(7)**: 1-17.

Padayachee B and Baijnath H. 2020. An updated comprehensive review of the medicinal, phytochemical and pharmacological properties of *Moringa oleifera. S Afr J Bot.*, **129**: 304-316.

Panigrahy D, Gilligan MM, Serhan CN and Kashfi K. 2021. Resolution of inflammation: an organizing principle in biology and medicine. *Pharmacol Ther.*, **227**: 1-16.

Pangalangan, RC. 2013. The domestic implementation of the international right to health: the Philippine experience. In: Zuniga JM, Marks AP and Gostin LO (eds.), **Advancing the Human Right to Health**. Oxford University Press, Oxford, England, pp.143.

Ridker PM. 2016. A test in context: high-sensitivity C-reactive protein. *J Am Coll Cardiol.*, **67(6)**: 712–723.

Sarrafzadegan N, Kelishadi R, Esmaillzadeh A, Mohammadifard N, Rabiei K, Roohafza H, Azadbakht L, Bahonar A, Sadri G, Amani A, Heidari S and Malekafzali H. 2009. Do lifestyle interventions work in developing countries? Findings from the Isfahan Healthy Heart Program in the Islamic Republic of Iran. *Bull World Health Organ.*, **87(1)**: 39-50.

Sayed AME, Omar FA, Emam MMA and Farag MA. 2022. UPLC-MS/MS and GC-MS based metabolites profiling of *Moringa oleifera* seed with its anti-*Helicobacter pylori* and anti-inflammatory activities. *Nat Prod Res.*, **36(24)**: 6433-6438.

Schneidman-Duhovny D, Dror O, Inbar Y, Nussinov R and Wolfson HJ. 2008. PharmaGist: a webserver for ligand-based pharmacophore detection. *Nucleic Acids Res.*, **36**: W223-W228.

Sharma V, Paliwal R, Janmeda P and Sharma S. 2012. Chemopreventive efficacy of *Moringa oleifera* pods against 7, 12-dimethylbenz[a]anthracene induced hepatic carcinogenesis in mice. *Asian Pac J Cancer Prev.*, **13(6)**: 2563-2569.

Shyu PT, Oyong GG and Cabrera EC. 2014. Cytotoxicity of probiotics from Philippine commercial dairy products on cancer cells and the effect on expression of *cfos* and *cjun* early apoptotic-promoting genes and Interleukin-1 β and Tumor Necrosis Factor-α proinflammatory cytokine genes. *Biomed Res Int.*, **491740**: 1-9.

Thompson PA, Khatami M, Baglole CJ, Sun J, Harris SA, Moon EY, Al-Mulla F, Al-Temaimi R, Brown DG, Colacci A, Mondello C, Raju J, Ryan EP, Woodrick J, Scovassi AI, Singh N, Vaccari M, Roy R, Forte S, Memeo L, Salem HK, Amedei A, Hamid RA, Lowe L, Guarnieri T and Bisson WH. 2015. Environmental immune disruptors, inflammation and cancer risk. *Carcinogenesis.*, **36(Suppl 1)**: S232–S253.

Trott O and Olson AJ. 2010. AutoDock Vina: improving the speed and accuracy of docking with a new scoring function, efficient optimization, and multithreading. *J Comput Chem.*, **31(2)**: 455-461.

Walker WH 2nd, Walton JC, DeVries AC and Nelson RJ. 2020. Circadian rhythm disruption and mental health. *Transl Psychiatry.*, **10(1)**: 1-13.

Veber DF, Johnson SR, Cheng HY, Smith BR, Ward KW and Kopple KD. 2002. Molecular properties that influence the oral bioavailability of drug candidates. *J Med Chem.*, **45(12)**: 2615-2623.

Velázquez-Zavala M, Peón-Escalante IE, Zepeda-Bautista R and Jiménez-Arellanes MA. 2016. Moringa (*Moringa oleifera* Lam.): potential uses in agriculture, industry and medicine. *Rev Chapingo Ser Hortic.*, **22(2)**: 95-116.

Xiong Y, Riaz Rajoka MS, Zhang M and He Z. 2022. Isolation and identification of two new compounds from the seeds of *Moringa oleifera* and their antiviral and anti-inflammatory activities. *Nat Prod Res.*, **36(4)**: 974-983.